



Research Article

Tracking the light-driven layer stacking of graphene oxide

Masaki Hada ^{a,b,*}, Satoshi Ohmura ^{c,1}, Yuki Yamamoto ^{a,1}, Yoshiya Kishibe ^a,
Wataru Yajima ^a, Ryo Shikata ^a, Tomohiro Iguchi ^d, Keishi Akada ^a, Shoji Yoshida ^a,
Jun-ichi Fujita ^a, Shin-ya Koshihara ^e, Yuta Nishina ^{d,f,**}

^a Faculty of Pure and Applied Sciences, University of Tsukuba, Tsukuba, 305-8573, Japan

^b Tsukuba Research Center for Energy Materials Science (TREMS), University of Tsukuba, Tsukuba, 305-8573, Japan

^c Faculty of Engineering, Hiroshima Institute of Technology, Hiroshima, 731-5193, Japan

^d Graduate School of Natural Science and Technology, Okayama University, Okayama, 700-8530, Japan

^e School of Science, Tokyo Institute of Technology, Tokyo, 152-8551, Japan

^f Research Core for Interdisciplinary Sciences, Okayama University, Okayama, 700-8530, Japan



ARTICLE INFO

Article history:

Received 6 April 2021

Received in revised form

16 July 2021

Accepted 20 July 2021

Available online 22 July 2021

Keywords:

Time-resolved electron diffraction

Ultrafast dynamics

Graphene oxide

π -stacking

Density functional calculations

ABSTRACT

Layer stacking of two-dimensional (2D) materials, such as graphene and transition metal dichalcogenides, is critical for controlling their physical and transport properties. By exploiting a specific stacking order, the electronic band structures of such 2D materials can be tuned, from which unusual and exotic properties may emerge. Graphene oxide (GO) undergoes layer stacking along with its photo- and thermal-induced reduction process; however, the underlying mechanism and dynamics during its layer stacking have not been revealed. In this study, we demonstrate time-resolved electron diffraction for monitoring the structural dynamics during the layer stacking of GO induced by ultraviolet photoexcitation. The experimental results accompanied by the density functional theory calculations reveal that AB stacking of graphitic domains of GO layers coincides within ~40 ps with photoinduced removal of the epoxy-oxygen from the basal plane of GO via the strong interactions between the GO layers.

© 2021 Elsevier Ltd. All rights reserved.

1. Introduction

As represented by the transition from graphene to graphite, layer stacking or the addition of an individual graphene layer completely modifies the material's electronic band structure [1–4]. Monolayer graphene has an electronic band structure with gapless Dirac cones [5,6], and stacking of graphene layers results in semiconductor and semimetal phases [7,8]. Recently, stacking graphene bilayers at a certain twist angle has been found to induce superconductor phase due to the interlayer interaction derived from the lattice mismatch between the layers [9–11]. Stacked layer graphene can be applied for field-effect transistors [12], lithium diffusion films in batteries [13], ultrahard carbon films [14,15], and catalytic fields [16]. Thus, layer stacking of graphene or other two-dimensional (2D) materials has attracted great fundamental and technological interest. Bilayer or few-layer graphene is fabricated

mainly by exfoliation of graphite [17,18] or by chemical vapor deposition [19]. Reduction of graphene oxide (GO) is an alternative technique to fabricate the stacked graphene [20–22]. However, there are several challenges in the fabrication of the stacked-layer graphene from GO. The mechanism underlying layer stacking of GO and even its structural dynamics remain to be fully elucidated. In this study, we demonstrate ultrafast time-resolved electron diffraction for capturing the onset of GO layer stacking induced by ultraviolet (UV) photoexcitation.

GO is a mass-producible derivative of graphene with several different oxygen functional groups on its basal plane and edge [23–27], and has been used for various applications, such as transparent conductive films [28], fibers [29], aerogels [30], membranes [31], energy storage devices [32], sensing devices [33], luminescent materials [34], fuel cells [35], biomaterials [36], liquid crystals [37], and polymer composites [38]. Reduction of GO is

* Corresponding author. Faculty of Pure and Applied Sciences, University of Tsukuba, Tsukuba, 305-8573, Japan.

** Corresponding author. Research Core for Interdisciplinary Sciences, Okayama University, Okayama, 700-8530, Japan.

E-mail addresses: hada.masaki.fm@u.tsukuba.ac.jp (M. Hada), nisina-y@cc.okayama-u.ac.jp (Y. Nishina).

¹ These authors equally contributed.

realized by removal of the oxygen functional groups [39]. Our previous study combined ultrafast time-resolved electron diffraction, ultrafast time-resolved mid-infrared vibrational spectroscopy, and time-dependent density functional theory (DFT) calculations to show that photoexcitation drives selective epoxy-oxygen removal from the basal plane of GO [40]. The selective removal of epoxy-oxygen is caused by the anti-bonding nature of epoxy-oxygen on the basal plane of GO in the photoexcited state. A previous report showed UV photoexcitation-induced structural dynamics on a single GO layer by analyzing the position shifts of the electron diffraction peaks from the $\{10\bar{1}0\}$ and $\{11\bar{2}0\}$ planes of GO. Herein, ultrafast time-resolved electron diffraction is intrinsically sensitive to the changes in the periodicity of molecules or molecular domains [41]; therefore, the structural dynamics of GO layer stacking can also be observed from the intensity changes of electron diffraction peaks. Interlayer interaction is quite weak in GO; therefore, GO layers are stacked independently from each other [42,43]. In contrast, reduced GO tends to undergo layer stacking with strong interlayer interactions [44]. Thus, in the present study, we focus on the intensity changes of these electron diffraction peaks to understand the structural dynamics of GO layer stacking (layer-to-layer dynamics) induced by UV photoexcitation.

2. Materials and methods

2.1. Preparation of GO films

GO was prepared using a modified Hummers' method [25,45]. The details of the synthesis of GO are given in Ref. [40]. We prepared two GO films, one for ultrafast time-resolved electron diffraction and the other for scanning electron microscopy (SEM). For ultrafast time-resolved electron diffraction, a 1 wt-% GO dispersion ($\text{H}_2\text{O}/\text{Solmix} = 1:1$) was spin-coated at a rotation speed of 2000 rpm onto an ultrathin (30-nm thickness) silicon nitride membrane. For SEM, a 0.2 wt-% GO dispersion (diluted dispersion) was spin-coated at a rotation speed of 2000 rpm onto a thermal SiO_2 substrate. In some very thin portions of the inhomogeneous GO film prepared from the diluted dispersion, monolayer and bilayer GO flakes were able to be observed. Fig. 1 shows the scanning electron micrograph (S-4800, Hitachi High-Tech Corp.) of a very thin portion of the GO film. The sizes of GO flakes are in the range of a few to tens of microns. The GO flakes of various sizes are stacked in layers.

2.2. Ultrafast time-resolved electron diffraction

Details of the ultrafast time-resolved electron diffraction setup are given elsewhere [46,47], and the experimental details are provided in a previous study [40]. The ultrafast time-resolved electron diffraction apparatus produced ultrashort (~ 1 ps) electron pulses. A 75-keV electrostatic field accelerated the employed electron beam. The repetition rate of electron pulses was 1 kHz. The GO film (~ 70 nm, approximately 60 GO layers) on the ultrathin silicon nitride substrate was excited by UV pulses (a wavelength of 266 nm) synchronized with the electron pulses.

2.3. Numerical details

We obtained the electronic states using the projector-augmented-wave (PAW) method [48,49] within the frozen core approximation in the framework of density functional theory (DFT). The generalized gradient approximation formulated by Perdew, Burke, and Ernzerhof (GGA-PBE) was used for the exchange-correlation potential [50]. The plane-wave cutoff energies for the

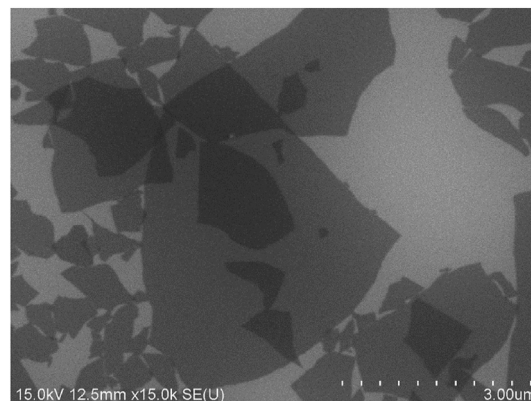


Fig. 1. Scanning electron micrograph of GO flakes.

pseudo-wavefunctions and pseudo charge density were 30 and 250 Ry, respectively. For valence electrons, we included 2s and 2p states of C and O. The energy functional was minimized using an iterative scheme based on the preconditioned conjugate-gradient method [51,52]. Total energy was converged to within a tolerance of

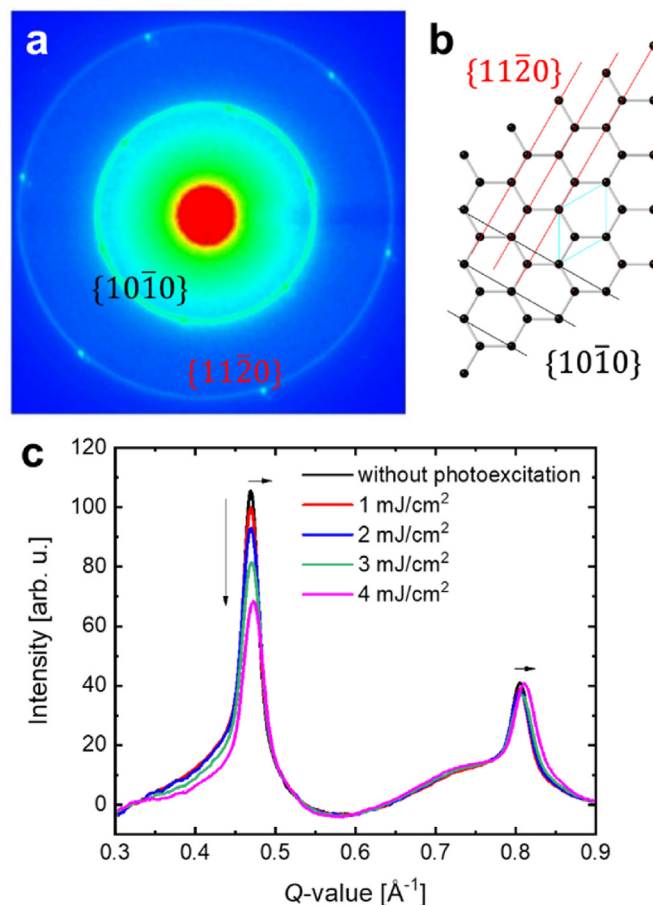


Fig. 2. (a) Electron diffraction pattern from GO. (b) The inset shows the geometric illustration of the $\{10\bar{1}0\}$ and $\{11\bar{2}0\}$ planes of graphene derived from unoxidized domains of GO. (c) The radial average of the electron diffraction patterns after UV photoexcitation at an incident fluence of 0–4 mJ/cm^2 . The horizontal arrows indicate the peak shifts, and the vertical arrow indicates the intensity change. (A colour version of this figure can be viewed online.)

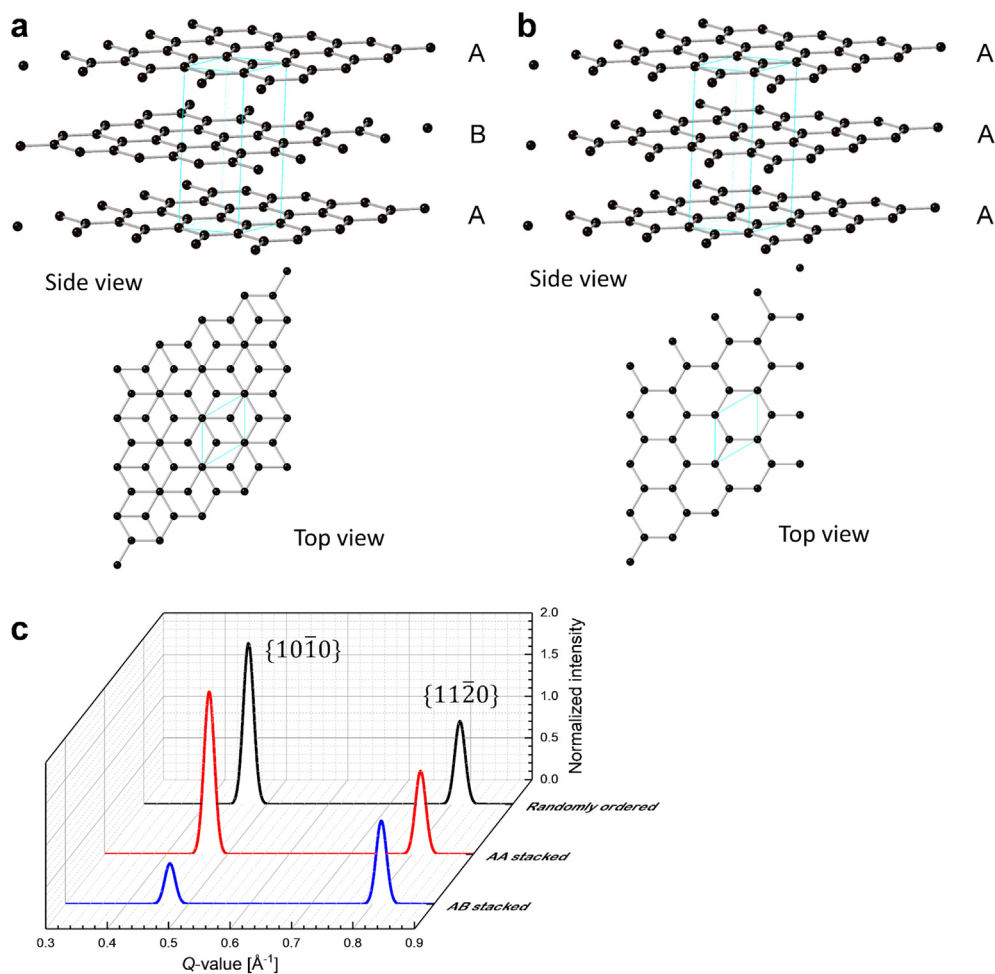


Fig. 3. (a, b) Schematic illustrations of graphene models stacked in AB and AA orders, respectively (side views and top views). (c) Calculated electron diffraction patterns from randomly ordered, AA stacked, and AB stacked graphene models. (A colour version of this figure can be viewed online.)

5.0×10^{-8} Ry/electron. The Γ point was used for Brillouin zone sampling. We applied van der Waals corrections to the GGA-PBE calculations by the DFT-D2 approach of Grimme [53], which is an empirical correction to standard DFT that takes into account dispersive interactions based on damped, atomic pairwise potentials. This approach has recently been applied to carbon systems, including graphite and graphene bilayers [54]. The simulation was performed using the highly parallelized plane-wave DFT program, for which implementation details can be found in Refs. [52,55–57]. To investigate electronic charges on each atom, we used the population analysis [58,59] by expanding the electronic wave functions in the atomic-orbital basis sets (Note S1).

3. Results and discussion

Fig. 2a shows the typical electron diffraction pattern from a GO film. The diffraction pattern shows the rings from the $\{10\bar{1}0\}$ and $\{11\bar{2}0\}$ planes of the GO framework. The geometries of the $\{10\bar{1}0\}$ and $\{11\bar{2}0\}$ planes of the graphene sheet are presented in Fig. 2b. As shown in the radial average of the electron diffraction pattern (Fig. 2c) after UV photoexcitation with 266-nm wavelength pulse, the Q-values of the $\{10\bar{1}0\}$ and $\{11\bar{2}0\}$ planes of GO were shifted higher, which reflects the lattice shrinkage of GO, i.e., the shrinkage of the average length of C–C bonds. The Q-value represents the reciprocal value of the lattice periodicity ($Q = 1/d$), where d is the

lattice periodicity. The C–C bonds of graphene correspond to conjugated double bonds. Once epoxy-oxygen is present on the basal plane of graphene, the two bonds of the conjugated double bonds become single bonds. The conjugated double bond is shorter than a single bond. The average length of C–C bonds decreases upon the removal of epoxy-oxygen. The average length of the C–C bonds of GO was 1.431 Å and shortened to 1.417 Å by epoxy-oxygen removal with UV photoexcitation at an incident fluence of 4 mJ/cm². In our previous report, time-dependent density functional theory calculations combined with time-resolved electron diffraction, time-resolved infrared vibrational spectroscopy, and X-ray photoelectron spectroscopy showed that the oxygen atoms of the epoxy-functional group (6–7%) with anti-bonding nature in the photoexcited state were removed from the basal plane of the GO layer [40]. Thus, the previous study effectively described the photoinduced structural dynamics within a single GO layer; however, it did not provide insights into the photoinduced layer-to-layer dynamics of GO. Spectroscopy is useful for understanding the reduction mechanism and structural dynamics within a single GO layer; however, it is difficult to elucidate the interlayer dynamics of GO with spectroscopic measurements. For example, Raman spectroscopy before and after UV photoexcitation (Figure S1) does not show any information about the changes in the interlayer structure of GO induced by UV photoexcitation.

Fig. 2c also shows the intensity changes of the electron diffraction peaks from the $\{10\bar{1}0\}$ and $\{11\bar{2}0\}$ planes of GO. The intensity

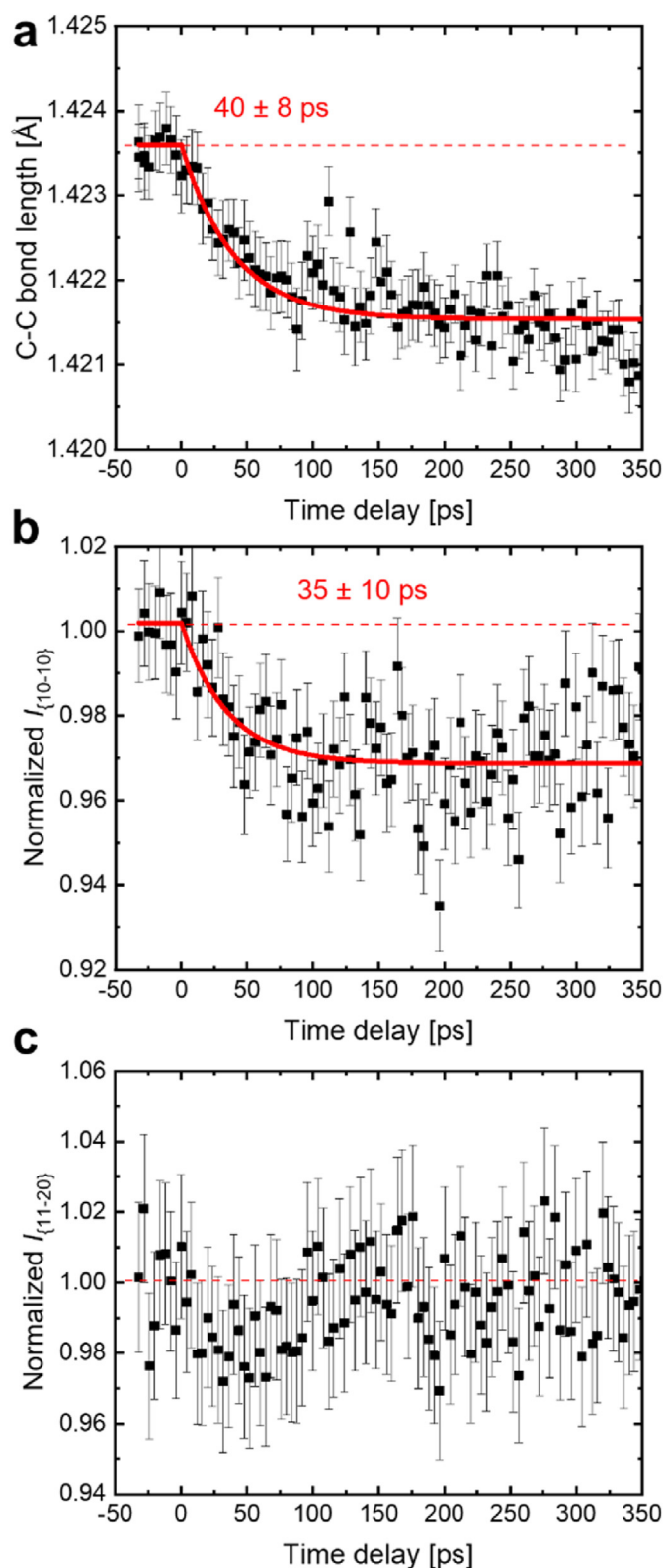


Fig. 4. (a) Temporal evolution of the change in the average C–C bond length of GO. Temporal evolution of the electron diffraction intensity from the $\{10\bar{1}0\}$ plane (b) and $\{11\bar{2}0\}$ plane (c). Red solid lines indicate the exponential fitting curves. The red dashed lines facilitate visual perception of the horizontal. (A colour version of this figure can be viewed online.)

of the diffraction peak from the $\{10\bar{1}0\}$ plane decreases by UV photoexcitation; in contrast, that from the $\{11\bar{2}0\}$ plane remains

constant after photoexcitation. More precisely, the intensity ratio ($I_{\{10\bar{1}0\}}/I_{\{11\bar{2}0\}}$) of the $\{10\bar{1}0\}$ and $\{11\bar{2}0\}$ diffraction rings is ~ 2 before photoexcitation, and it decreases to less than two after photoexcitation above the incident fluence of 2–3 mJ/cm².

The experimentally obtained intensity changes of the diffraction peaks from the $\{10\bar{1}0\}$ and $\{11\bar{2}0\}$ planes of GO can be estimated by the kinematic theory of diffraction based on graphene models. Fig. 3a and b shows the AB stacking and AA stacking of graphene layers, respectively. Randomly ordered graphene models are shown in the supporting information in more detail (Figure S2). The calculated electron diffraction patterns from randomly ordered, AB stacked, and AA stacked graphene layers are presented in Fig. 3c. The electron diffraction patterns are calculated based on kinematic theory [60]. The profiles of the calculated electron diffraction patterns from the randomly ordered graphene layers and the AA stacked graphene layers are identical, which can be clearly understood by viewing the AA stacked graphene layer from above (Fig. 3b). As shown in Fig. 3c, the intensity of the diffraction peak from the $\{10\bar{1}0\}$ plane of AB stacked graphene layers is four times lower than those of AA stacked or randomly ordered graphene layers. On the other hand, the diffraction peaks from the $\{11\bar{2}0\}$ plane of randomly ordered, AB stacked, and AA stacked graphene layers share the same intensity. The ratio of the $\{10\bar{1}0\}$ and $\{11\bar{2}0\}$ diffraction intensities ($I_{\{10\bar{1}0\}}/I_{\{11\bar{2}0\}}$) of randomly ordered graphene or AA stacked graphene is 2. The value for AB stacked graphene is 0.5. Thus, GO is randomly ordered on the substrate for electron diffraction before photoexcitation. The experimentally obtained decrease in intensity ratio by UV photoexcitation (Fig. 2c) would suggest a change in the stacking order of GO from random order to AB stacked order.

Noting the structural dynamics of the stacking order of GO upon the UV photoexcitation can lead to further understanding of its mechanism. We discuss the structural dynamics of GO from the changes in the electron diffraction patterns following UV photoexcitation at an incident fluence of 2 mJ/cm². The changes in the average C–C bond length of GO can be calculated from the shifts of the diffraction peaks from the $\{10\bar{1}0\}$ and $\{11\bar{2}0\}$ planes of GO. Fig. 4a shows the temporal evolution of the average C–C bond length of GO. The time constant of the change in the average C–C bond length of GO is 40 ± 8 ps, as shown in a previous report. This lattice shrinkage is caused by removal of epoxy-oxygen from the basal plane of GO. Fig. 4b and c shows the temporal evolutions of the normalized intensity changes of the $\{10\bar{1}0\}$ and $\{11\bar{2}0\}$ diffraction rings of GO, respectively. The electron diffraction intensity from the $\{10\bar{1}0\}$ plane decreases by approximately 3% by UV photoexcitation with a time constant of 35 ± 10 ps (Fig. 4b). The time constant of the intensity decrease corresponds well to that of the change in the average C–C bond length of GO. In contrast, the electron diffraction intensity from the $\{11\bar{2}0\}$ plane does not change upon UV photoexcitation (Fig. 4c). This tendency is also explained by the calculated electron diffraction patterns shown in Fig. 3c, where the randomly ordered graphene is transformed into locally AB stacked graphene by UV photoexcitation. The correspondence of the time constant of the shrinkage of the average C–C bond length induced by the removal of epoxy-functional groups and that of change in layer order from randomly ordered GO to AB stacked GO suggests that the epoxy-oxygen removal and change in layer stacking have a strong correlation. The correlation can be quantitatively analyzed by comparing the ratio of the removed epoxy-oxygen and the degree of the AB stacking of the GO layers. According to a previous study, the average length of the C–C bonds shortens by 0.014 Å (from 1.431 Å to 1.417 Å) when 6–7% of epoxy-oxygen is removed from the basal plane of the GO layer [40]. Fig. 4a

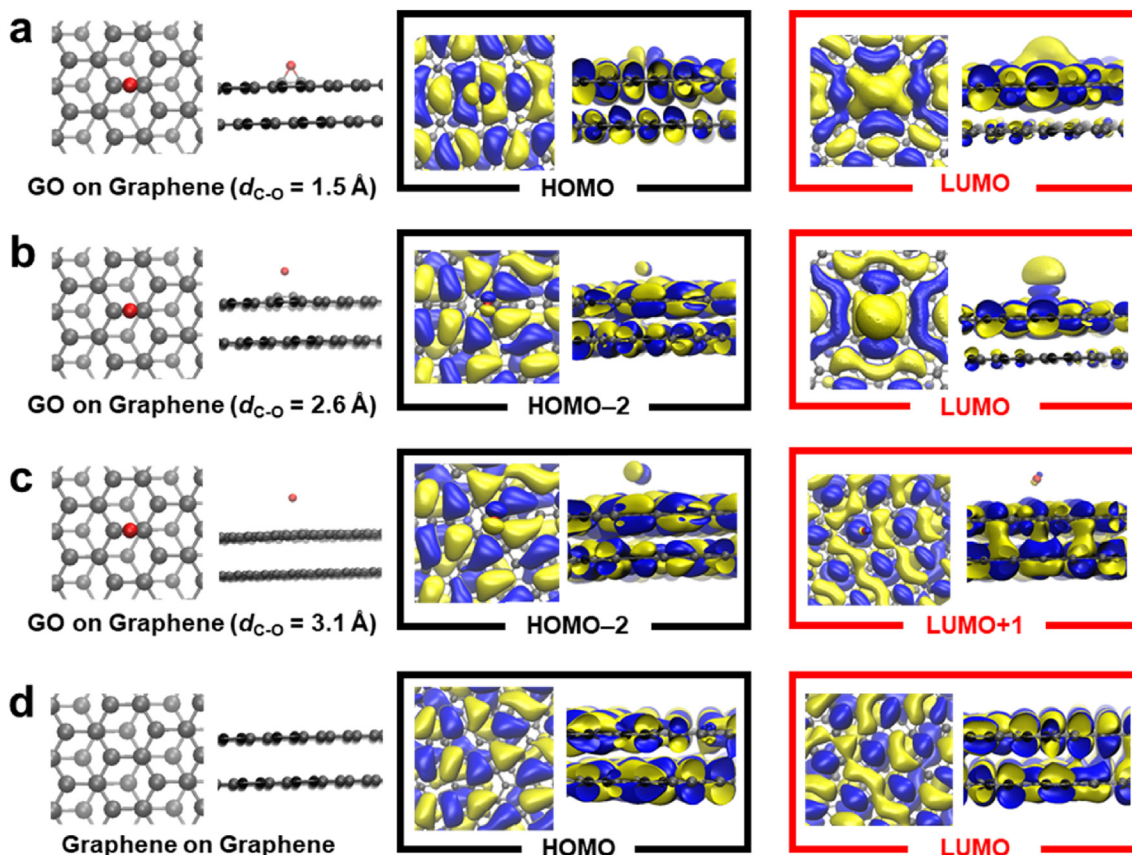


Fig. 5. Model bilayer graphene structures (top and side views) with epoxy-functional groups at C–O distances of 1.5 Å (a), 2.6 Å (b), and 3.1 Å (c), and without epoxy-functional groups (d). The right panels show the HOMOs and LUMOs of the graphene models. (A colour version of this figure can be viewed online.)

shows that the average length of the C–C bonds shrinks by 0.0021 Å with photoexcitation by a single UV pulse at an incident fluence of 2 mJ/cm², which suggests that ~1 % of epoxy-oxygen moves away from the basal plane of the GO layer with a single UV pulse. On the other hand, as shown in Fig. 3c, the electron diffraction intensity from the {10 $\bar{1}$ 0} plane would decrease by 75 % when the randomly ordered GO layers have fully transformed into AB stacked GO layers. The experimental result that the electron diffraction intensity from the {10 $\bar{1}$ 0} plane decreases by approximately 3 % upon UV photoexcitation suggests that ~4 % of randomly ordered GO layers partially change into AB stacked GO layers upon irradiation by a single UV pulse. Thus, the adjacent 4 % carbon atoms with epoxy-oxygen locally form AB stacking layers upon ~1 % epoxy-oxygen removal from the basal plane of GO.

To understand the causality between epoxy-oxygen removal and layer stacking, we performed DFT calculations. Fig. 5a–d shows the model bilayer graphene structures with and without the epoxy-functional group, i.e., bilayer GO models. Each layer consists of an 8 × 8 graphene supercell (128 carbon atoms) in the periodic boundary condition of the hexagonal net (Figure S3). In z-direction, the periodic boundary condition is employed with a cell of a dimension of 25 Å, which is large enough to avoid the interaction between periodic images of layers. In the initial structure optimization, iterations were repeated until the atomic forces reached values lower than 0.02 eV/Å. To generate the layer without oxygen, structural optimization was performed locally around carbon atoms used to bond to an oxygen atom starting from the same atomic configuration of GO. The distances between layers with and without epoxy-oxygen are 3.5 and 3.4 Å, respectively. The highest

occupied molecular orbitals (HOMOs) and lowest unoccupied molecular orbitals (LUMOs) of the corresponding bilayer GO models are shown in the right panels. The HOMOs and LUMOs of the bilayer GO models are shown in more detail in Figure S4. Each structure of the bilayer GO model features an epoxy-functional group on its upper layer. The average distances between the two nearest carbon atoms and the oxygen atom (C–O distances) are 1.5, 2.6, and 3.1 Å. As shown in Fig. 5a and b, the wave function is attracted by the epoxy-functional group when the epoxy-functional group is close to the graphene layer. The electron probability density is the squared amplitude of the wave function. The wave function of the bilayer GO model with a C–O distance of 3.1 Å (Fig. 5c) is similar to that without an epoxy-functional group (Fig. 5d), which indicates that the interaction between two graphene layers of the GO model is also similar to that of the graphene bilayer. In these configurations, the wave functions in the HOMO–2 of two graphene layers of the GO model (Fig. 5c) is close to each other. Thus, the result from the DFT calculation reflects that the removal of the epoxy-functional group from the basal plane of GO strongly influences the stacking of GO.

We performed additional quantitative analyses of the DFT calculations. The differential electronic charge between the upper and lower graphene layers in Fig. 6a is defined to be Q_{diff} by the following equation:

$$Q_{diff} = \sum Q(carbon)_{lower} - \sum Q(carbon)_{upper}, \quad (1)$$

where $Q(carbon)_{lower}$ and $Q(carbon)_{upper}$ are the electronic charges of the carbon atoms in the lower graphene and in the upper

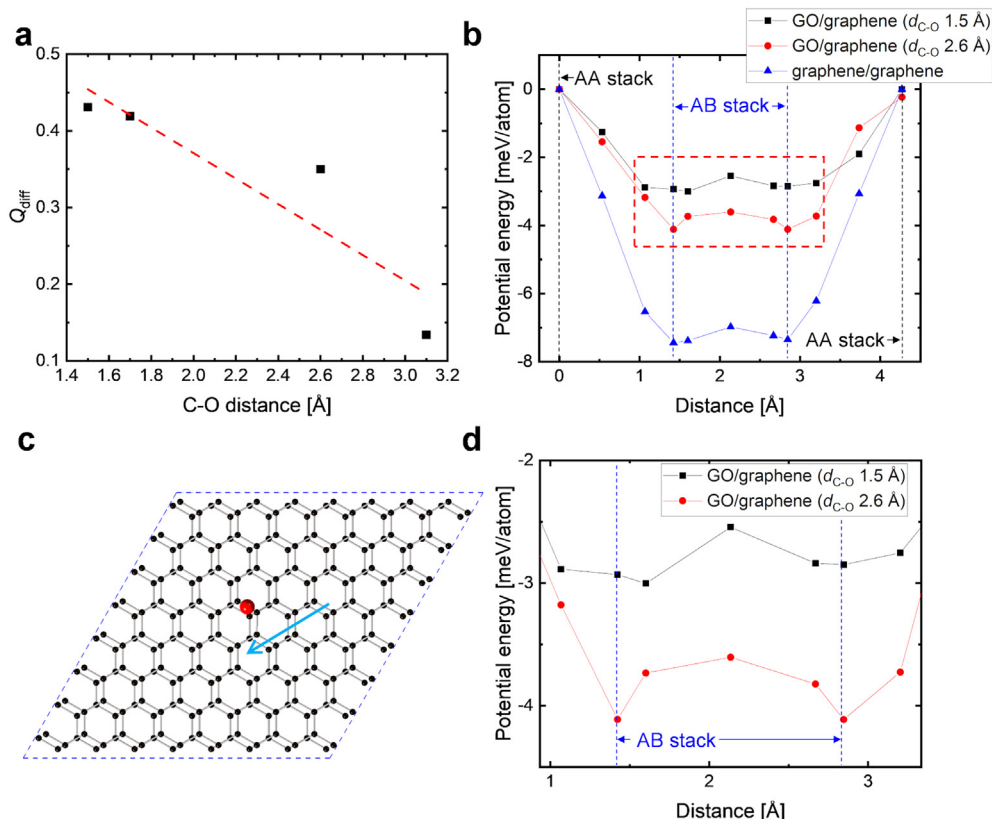


Fig. 6. (a) The differential electronic charge between the upper and lower graphene layers, Q_{diff} , as a function of C–O distance. (b) Potential energy curves of the bilayer GO models with C–O distances of 1.5 and 2.6 Å and without epoxy-oxygen. The origin of the axis representing energy is taken to be the energy at the AA stacking. (c) The direction of the upper layer sliding. The horizontal axis of (b) is the position of the upper layer sliding in the $[10\bar{1}0]$ direction (the blue arrow). (d) Enlarged view of the red dashed square shown in (b). (A colour version of this figure can be viewed online.)

graphene, respectively. The positive value of Q_{diff} indicates that the electronic charge is localized at the oxygen site. Fig. 6a shows Q_{diff} as a function of a C–O distance. As shown in the figure, Q_{diff} has a positive value (0.4–0.5 elementary charges) with the C–O distance of ~ 1.5 Å, and it decreases as the C–O distance increases. At C–O distance over ~ 3.1 Å, Q_{diff} is approximately 0.1 elementary charges, which is close to the configuration of bilayer graphene. The potential energy curves of the bilayer GO models with C–O distances of 1.5 and 2.6 Å and without an epoxy-functional group are shown in Fig. 6b. As shown in Fig. 6c, the upper layer slide in the $[10\bar{1}0]$ direction, where we define the distance of 0 Å as the AA stacked bilayer GO. The distances equal to 0 Å and 4.27 Å correspond to AA stacked bilayer GO (black dashed lines), and the distances equal to 1.42 Å and 2.85 Å correspond to AB stacked bilayer GO (blue dashed lines). The potential energy curve of the model without the epoxy-functional group has minima at the position of the AB stacked bilayer. As shown in the enlarged view (Fig. 6d), the potential energy curve of the bilayer GO model with C–O distances of 1.5 Å is relatively flat without potential minima around the position of AB-stacking; in contrast, that of the bilayer GO model with C–O distances of 2.6 Å exhibits potential minima at the position of the AB stacked bilayer GO. This calculation result suggests that elongation of the distance between the epoxy-functional group and the basal plane of GO creates the potential minimum at the position of the AB stacked bilayer GO and enhances the interaction between the GO layers. The relationship of potential energy to C–O distance in AB stacking and AA stacking also supports the posited enhancement of AB stacking by epoxy-oxygen removal (Figure S5). The other possible configurations, such as bilayer GO model with

the hydroxyl-functional groups and trilayer GO model, are shown in Figures S6 and S7; all of them also suggest the enhancement of AB stacking after the removal of epoxy-oxygen.

4. Conclusion

In summary, the ultrafast structural dynamics of the stacking of GO induced by UV photoexcitation were investigated using a combination of ultrafast time-resolved electron diffraction and DFT calculations. Randomly ordered GO layers become stacked in AB order simultaneously with removal of the epoxy-functional group on the basal plane of GO. The wave function of the bilayer GO model approaches that without an epoxy-functional group with increasing C–O distance. The stacking of GO layers was caused by the strong interaction between layers. The elucidated mechanism of GO layer stacking may allow tuning of the desired stacking order of graphene or functionalized graphene layers and thus realize control of their physical and transport properties, expanding the application scope of 2D materials [61].

CRedit authorship contribution statement

Masaki Hada: Conceptualization, Methodology, Formal analysis, Investigation, Writing – original draft. **Satoshi Ohmura:** Methodology, Software, Formal analysis, Investigation, Writing – original draft. **Yuki Yamamoto:** Formal analysis, Investigation, Writing – original draft. **Yoshiya Kishibe:** Investigation. **Wataru Yajima:** Investigation. **Ryo Shikata:** Investigation. **Tomohiro Iguchi:** Investigation. **Keishi Akada:** Investigation. **Shoji Yoshida:**

Investigation. **Jun-ichi Fujita**: Data curation, Investigation. **Shin-ya Koshihara**: Data curation, Writing – review & editing. **Yuta Nishina**: Conceptualization, Investigation, Resources, Writing – review & editing.

Declaration of competing interest

The authors declare that they have no known competing financial interests or personal relationships that could have appeared to influence the work reported in this paper.

Acknowledgments

This work was financially supported by Kakenhi Grants-in-Aid (Nos. JP18H05208, JP19H00847, JP20H01832, and JP20H04657) and JST CREST (No. JPMJCR18R3). This work was also supported by the Leading Initiative for Excellent Young Researchers of the Ministry of Education, Culture, Sports, Science and Technology (MEXT), Japan. Computations were carried out using the computer facilities at the Research Institute for Information Technology, Kyushu University and at the Supercomputer Center, Institute for Solid State Physics, University of Tokyo.

Appendix A. Supplementary data

Supplementary data to this article can be found online at <https://doi.org/10.1016/j.carbon.2021.07.058>.

References

- [1] P.R. Wallace, The band theory of graphite, *Phys. Rev.* 71 (1947) 622.
- [2] J.C. Slonczewski, P.R. Weiss, Band structure of graphite, *Phys. Rev.* 109 (1958) 272–279.
- [3] F. Guinea, A.H. Castro Neto, N.M.R. Peres, Electronic states and Landau levels in graphene stacks, *Phys. Rev. B* 73 (2006) 245426.
- [4] A.K. Geim, K.S. Novoselov, The rise of graphene, *Nat. Mater.* 6 (2007) 183–191.
- [5] K.S. Novoselov, A.K. Geim, S.V. Morozov, D. Jiang, M.I. Katsnelson, I.V. Grigorieva, S.V. Dubonos, A.A. Firsov, Two-dimensional gas of massless Dirac fermions in graphene, *Nature* 438 (2005) 197–200.
- [6] Y. Zhang, J.W. Tan, H.L. Stormer, P. Kim, Experimental observation of the quantum hall effect and Berry's phase in graphene, *Nature* 438 (2005) 201–204.
- [7] Y. Zhang, T. Tang, C. Girit, Z. Hao, M.C. Martin, A. Zettl, M.F. Crommie, Y.R. Shen, F. Wang, Direct observation of a widely tunable bandgap in bilayer graphene, *Nature* 459 (2009) 820–823.
- [8] W. Bao, L. Jing, J. Velasco, Y. Lee, G. Liu, D. Tran, B. Standley, M. Aykol, S.B. Cronin, D. Smirnov, M. Koshino, E. McCann, M. Bockrath, C.N. Lau, Stacking-dependent band gap and quantum transport in trilayer graphene, *Nat. Phys.* 7 (2011) 948–952.
- [9] Y. Cao, V. Fatemi, S. Fang, K. Watanabe, T. Taniguchi, E. Kaxiras, P. Jarillo-Herrero, Unconventional superconductivity in magic-angle graphene superlattices, *Nature* 556 (2018) 43–50.
- [10] Y. Cao, V. Fatemi, A. Demir, S. Fang, S.L. Tomarken, J.Y. Luo, J.D. Sanchez-Yamagishi, K. Watanabe, T. Taniguchi, E. Kaxiras, R.C. Ashoori, P. Jarillo-Herrero, Correlated insulator behaviour at half-filling in magic-angle graphene superlattices, *Nature* 556 (2018) 80–84.
- [11] M. Yankowitz, S. Chen, H. Polshyn, Y. Zhang, K. Watanabe, T. Taniguchi, D. Graf, A.F. Young, C.R. Dean, Tuning superconductivity in twisted bilayer graphene, *Science* 363 (2019) 1059–1064.
- [12] F. Schwierz, Graphene transistors, *Nat. Nanotechnol.* 5 (2010) 487–496.
- [13] M. Kühne, F. Paolucci, J. Popovic, P.M. Ostrovsky, J. Maier, J.H. Smet, Ultrafast lithium diffusion in bilayer graphene, *Nat. Nanotechnol.* 12 (2017) 895–900.
- [14] Y. Gao, T. Cao, F. Cellini, C. Berger, W.A. De Heer, E. Tosatti, E. Riedo, A. Bongiorno, Ultrahard carbon film from epitaxial two-layer graphene, *Nat. Nanotechnol.* 13 (2018) 133–138.
- [15] F. Zhao, A. Afandi, R.B. Jackman, Graphene diamond-like carbon films heterostructure, *Appl. Phys. Lett.* 106 (2015), 102108.
- [16] V. Georgakilas, J.N. Tiwari, K.C. Kemp, J.A. Perman, A.B. Bourlinos, K.S. Kim, R. Zboril, Noncovalent functionalization of graphene and graphene oxide for energy materials, biosensing, catalytic, and biomedical applications, *Inside Chem.* 116 (2016) 5464–5519.
- [17] K.S. Novoselov, A.K. Geim, S.V. Morozov, D. Jiang, Y. Zhang, S.V. Dubonos, I.V. Grigorieva, A.A. Firsov, Electric field effect in atomically thin carbon films, *Science* 306 (2004) 666–669.
- [18] K.S. Novoselov, D. Jiang, F. Schedin, T.J. Booth, V.V. Khotkevich, S.V. Morozov, A.K. Geim, Two-dimensional atomic crystals, *Proc. Natl. Acad. Sci. U.S.A.* 102 (2005) 10451–10453.
- [19] K.S. Kim, Y. Zhao, H. Jang, S.Y. Lee, J.M. Kim, K.S. Kim, J. Ahn, P. Kim, J. Choi, B.H. Hong, Large-scale pattern growth of graphene films for stretchable transparent electrodes, *Nature* 457 (2009) 706–710.
- [20] S. Pei, H.M. Cheng, The reduction of graphene oxide, *Carbon* 50 (2012) 3210–3228.
- [21] Y. Yoon, K. Lee, C. Baik, H. Yoo, M. Min, Y. Park, S.M. Lee, H. Lee, Anti-solvent derived non-stacked reduced graphene oxide for high performance supercapacitors, *Adv. Mater.* 25 (2013) 4437–4444.
- [22] N. Morimoto, T. Kubo, Y. Nishina, Tailoring the oxygen content of graphite and reduced graphene oxide for specific applications, *Sci. Rep.* 6 (2016) 21715.
- [23] L. Staudenmaier, Verfahren zur Darstellung der Graphitsäure, *Ber. Dtsch. Chem. Ges.* 31 (1898) 1481–1487.
- [24] B.C. Brodie, On the atomic weight of graphite, *Trans. R. Soc.* 149 (1859) 249–259.
- [25] W.S. Hummers, R.E. Offeman, Preparation of graphitic oxide, *J. Am. Chem. Soc.* 80 (1958) 1339.
- [26] H. He, J. Klinowski, M. Forster, A.A. Lerf, New structural model for graphite oxide, *Chem. Phys. Lett.* 287 (1998) 53–56.
- [27] A.M. Dimiev, S. Eglar (Eds.), *Graphene Oxide: Fundamentals and Applications*, John Wiley & Sons, Incorporated, 2017.
- [28] Q. Zheng, Z. Li, J. Yang, J.-K. Kim, Graphene oxide-based transparent conductive film, *Prog. Mater. Sci.* 64 (2014) 200–247.
- [29] F. Meng, W. Lu, Q. Li, J.H. Byun, Y. Oh, T.W. Chou, Graphene-based fibers: a review, *Adv. Mater.* 27 (2015) 5113–5131.
- [30] G. Gorgolis, C. Galiotis, Graphene aerogels: a review, *2D Mater.* 4 (2017), 032001.
- [31] R.K. Joshi, S. Alwarappan, M. Yoshimura, V. Sahajwalla, Y. Nishina, Graphene oxide: the new membrane material, *Appl. Mater. Today* 1 (2015) 1–12.
- [32] R. Khan, Y. Nishina, Covalent functionalization of carbon materials with redox-active organic molecules for energy storage, *Nanoscale* 13 (2021) 36–50.
- [33] J. Liu, Z. Liu, C.J. Barrow, W. Yang, Molecularly engineered graphene surfaces for sensing applications: a review, *Anal. Chim. Acta* 859 (2015) 1–19.
- [34] Q. Mei, B. Liu, G. Han, R. Liu, M.Y. Han, Z. Zhang, Graphene oxide: from tunable structures to diverse luminescence behaviors, *Adv. Sci.* 6 (2019), 1900855.
- [35] R. Yadav, A. Subhash, N. Chemmenchery, B. Kandasubramanian, Graphene and graphene oxide for fuel cell technology, *Ind. Eng. Chem. Res.* 57 (2018) 9333–9350.
- [36] M.Z.I. Nizami, S. Takashiba, Y. Nishina, Graphene oxide: a new direction in dentistry, *Appl. Mater. Today* 19 (2020), 100576.
- [37] R. Narayan, J.E. Kim, J.Y. Kim, K.E. Lee, S.O. Kim, Graphene oxide liquid crystals: discovery, evolution and applications, *Adv. Mater.* 28 (2016) 3045–3068.
- [38] W.K. Chee, H.N. Lim, N.M. Huang, I. Harrison, Nanocomposites of graphene/polymers: a review, *RSC Adv.* 5 (2015) 68014–68051.
- [39] A. Bianco, H.-M. Cheng, T. Enoki, Y. Gogotsi, R.H. Hurt, N. Koratkar, T. Kyotani, M. Monthieux, C.R. Park, J.M.D. Tascon, J. Zhang, All in the graphene family – a recommended nomenclature for two-dimensional carbon materials, *Carbon* 65 (2013) 1–6.
- [40] M. Hada, K. Miyata, S. Ohmura, Y. Arashida, K. Ichiyangagi, I. Katayama, T. Suzuki, W. Chen, S. Mizote, T. Sawa, T. Yokota, T. Seki, J. Matsuo, T. Tokunaga, C. Itoh, K. Tsuruta, R. Fukuya, S. Nozawa, S. Adachi, J. Takeda, K. Onda, S. Koshihara, Y. Hayashi, Y. Nishina, Selective reduction mechanism of graphene oxide driven by the photon mode versus the thermal mode, *ACS Nano* 13 (2019) 10103–10112.
- [41] M. Hada, Y. Nishina, T. Kato, Exploring structures and dynamics of molecular assemblies: ultrafast time-resolved electron diffraction measurements, *Acc. Chem. Res.* 54 (2021) 731–743.
- [42] K.A. Mkhoyan, A.W. Contryman, J. Silcox, D.A. Stewart, G. Eda, C. Mattevi, S. Miller, M. Chhowalla, Atomic and electric structure of graphene-oxide, *Nano Lett.* 9 (2009) 1058–1063.
- [43] X. Díez-Betriu, F.J. Mompeán, C. Munuera, J. Rubio-Zuazo, R. Menéndez, G.R. Castro, A. Andrés, Graphene-oxide stacking and defects in few-layer films: impact of thermal and chemical reduction, *Carbon* 80 (2014) 40–49.
- [44] C. Gómez-Navarro, J.C. Meyer, R.S. Sundaram, A. Chuvilin, S. Kurasch, M. Burghard, K. Kern, U. Kaiser, Atomic structure of reduced graphene oxide, *Nano Lett.* 10 (2010) 1144–1148.
- [45] N. Morimoto, H. Suzuki, Y. Takeuchi, S. Kawaguchi, M. Kunisu, C.W. Bielawski, Y. Nishina, Real-time, in situ monitoring of the oxidation of graphite: lessons learned, *Chem. Mater.* 29 (2017) 2150–2156.
- [46] M. Hada, S. Saito, R. Sato, K. Miyata, Y. Hayashi, Y. Shigeta, K. Onda, Novel techniques for observing structural dynamics of photoresponsive liquid crystals, *JoVE* 135 (2018), e57612.
- [47] M. Hada, D. Yamaguchi, T. Ishikawa, T. Sawa, K. Tsuruta, K. Ishikawa, S. Koshihara, Y. Hayashi, T. Kato, Ultrafast isomerization-induced cooperative motions to higher molecular orientation in smectic liquid-crystalline azobenzene molecules, *Nat. Commun.* 10 (2019) 4159.
- [48] P.E. Blöchl, Projector augmented-wave method, *Phys. Rev. B* 50 (1994) 17953–17979.
- [49] G. Kresse, D. Joubert, From ultrasoft pseudopotentials to the projector augmented-wave method, *Phys. Rev. B* 59 (1999) 1758–1775.
- [50] J.P. Perdew, K. Burke, M. Ernzerhof, Generalized gradient approximation made simple, *Phys. Rev. Lett.* 77 (1996) 3856–3868.
- [51] G. Kresse, J. Hafner, Ab-initio molecular-dynamics simulation of the liquid-

- metal amorphous-semiconductor transition in germanium, *Phys. Rev. B* 49 (1994) 14251–14269.
- [52] F. Shimojo, R.K. Kalia, A. Nakano, P. Vashishta, Linear-scaling density-functional-theory calculations of electronic structure based on real-space grids: design, analysis, and scalability test of parallel algorithms, *Comput. Phys. Commun.* 140 (2001) 303–314.
- [53] S. Grimme, Semiempirical GGA-type density functional constructed with a long-range dispersion correction, *J. Comput. Chem.* 27 (2006) 1787–1799.
- [54] A. Impellizzeri, P. Briddon, C.P. Ewels, Stacking- and chirality-dependent collapse of single-walled carbon nanotubes: a large-scale density-functional study, *Phys. Rev. B* 100 (2019), 115410.
- [55] F. Shimojo, Y. Zempo, K. Hoshino, M. Watabe, First-principles molecular-dynamics simulation of expanded liquid rubidium, *Phys. Rev. B* 52 (1995) 9320–9329.
- [56] F. Shimojo, S. Hattori, R.K. Kalia, M. Kunaseth, W. Mou, A. Nakano, K. Nomura, S. Ohmura, P. Rajak, K. Shimamura, P. Vashishta, A divide-conquer-recombine algorithmic paradigm for large spatiotemporal quantum molecular dynamics simulations, *J. Chem. Phys.* 140 (2014), 18A529-1-14.
- [57] F. Shimojo, S. Fukushima, H. Kumazoe, M. Misawa, S. Ohmura, P. Rajak, K. Shimamura, L. Bassman, S. Tiwari, R.K. Kalia, A. Nakano, P. Vashishta, QXMD: an open-source program for nonadiabatic quantum molecular dynamics, *Software* 10 (2019), 100307.
- [58] R.S. Mulliken, Electronic population analysis on LCAO-MO molecular wave functions. II. Overlap populations, bond orders, and covalent bond energies, *J. Chem. Phys.* 23 (1955) 1841–1846.
- [59] F. Shimojo, A. Nakano, R.K. Kalia, P. Vashishta, Electronic processes in fast thermite chemical reactions: a first-principles molecular dynamics study, *Phys. Rev. E* 77 (2008), 066103.
- [60] CrystalMaker® and CrystalDiffract®, CrystalMaker Software Limited; available at: <http://crystalmaker.com/index.html> (accessed Jan. 25, 2021).
- [61] A. Ambrosi, C.K. Chua, A. Bonanni, M. Pumera, Electrochemistry of graphene and related materials, *Chem. Rev.* 114 (2014) 7150–7188.